

# Transient shear banding in entangled polymers: a study using the Rolie-Poly model

J. M. Adams,<sup>1</sup> S. M. Fielding,<sup>2</sup> and P. D. Olmsted<sup>3</sup>

<sup>1</sup>*SEPNet and the Department of Physics, University of Surrey, Guildford, GU2 7HX, UK*

<sup>2</sup>*Department of Physics, Durham University, Science Laboratories, South Road, Durham, DH1 3LE, UK*

<sup>3</sup>*School of Physics & Astronomy, University of Leeds, Leeds, LS2 9JT, UK*

(Dated: 3 June 2011)

Spatially inhomogeneous shear flow occurs in entangled polymer solutions, both as steady state shear banding and transiently after a large step strain or during start up to a steady uniform shear rate. Theoretically, steady state shear banding is a hallmark of models with a non-monotonic constitutive relation between total shear stress and applied shear rate, but transient banding is sometimes seen in fluids that do *not* shear band at steady state. We model this behavior using the diffusive Rolie-Poly model in a Newtonian solvent, whose steady state constitutive behavior can be monotonic or non-monotonic depending on the degree of convective constraint release (CCR). We study monotonic steady state constitutive behaviour. Linear stability analysis of start up to a sufficiently high shear rate shows that spatial fluctuations are unstable at early times. There is a strong correlation between this instability and the negative slope of the (time dependent) constitutive curve. If the time integral of the most unstable eigenvalue is sufficiently large then the system exhibits transient shear bands that later vanish in steady state. We show how perturbations, due to fluctuations or the inhomogeneous stresses, can trigger this instability. This transient behavior is similar to recent observations in entangled polymer solutions.

## I. INTRODUCTION

The original theory of Doi and Edwards (1989) predicts shear banding in entangled polymers, when the shear rate exceeds the reciprocal of the timescale  $\tau_d$  for one-dimensional diffusion (reptation) within an effective mean field tube of constraints from the surrounding molecules. For shear rates  $\dot{\gamma} \gtrsim 1/\tau_d$ , DE theory predicts a decreasing shear stress  $\sigma_{xy}(\dot{\gamma})$  due to enhanced tube alignment, and thus leads to a non-monotonic constitutive curve  $\sigma_{xy}(\dot{\gamma})$  and an instability to an inhomogeneous state in which two states, or ‘shear bands’, of different viscosity and molecular alignment coexist (McLeish and Ball, 1986). However, banding was not inferred at that time in polymers; for example, the apparent viscosity measurements of Menezes and Graessley (1982) on entangled polymers are consistent with a weakly increasing shear stress for  $\dot{\gamma}\tau_d > 1$ , rather than the stress plateau that is expected from banding. By contrast, banding is prevalent in wormlike micelles (Rehage and Hoffmann, 1991; Berret, 2005; Cates and Fielding, 2006; Olmsted, 2008). This was explained by Cates (1990), who combined reptation with micellar breaking to predict shear banding at stresses and shear rates in good qualitative agreement with experiments (Spenley *et al.*, 1993). It is now realized that a strictly constant stress plateau is not obtained for banding in a curved geometry, such as cone and plate or cylindrical Couette fixtures (Olmsted *et al.*, 2000), so the results of Menezes and Graessley (1982) may in fact be consistent with shear banding.

Discrepancies with DE theory have existed virtually since the theory’s inception (Fukuda *et al.*, 1975), par-

ticularly in the response of highly entangled polymeric fluids to a step strain. Osaki and Kurata (1980) and Vrentas and Graessley (1982) observed stress relaxation that was much faster than predicted by DE theory. This is particularly prevalent for entanglement numbers  $Z \gtrsim 60$  for relaxation after large step strain (Osaki, 1993), and has been termed anomalous or “type C” relaxation (Osaki, 1993; Venerus, 2005). Marrucci and Grizzuti (1983) (MG) pointed out that the DE theory contains an elastic instability; they showed that the free energy can be a convex function of strain for large enough step strain (for  $\dot{\gamma}\tau_d \gg 1$ ). This would then lead to an elastic instability and thus inhomogeneous (shear banding) behavior. They showed how this instability can persist even when one includes relaxation. McLeish and Ball (1986) later suggested that the DE theory could explain the measurements of the spurt effect by Vinogradov (1973), in terms of the inherent instability to shear banding. Kolkka *et al.* (1988) used the Johnson-Segalman model to study the nature of mechanical instabilities inherent in fluid with a non-monotonic constitutive relation. It was later demonstrated that wall slip plays a major role in spurt (Wang, 1999; Denn, 2001). Morrison and Larson (1992) tested Marrucci and Grizzuti’s idea by using entangled solutions at different concentrations to mimic the effect of relaxation. They concluded that the Marrucci-Greco mechanism gives a qualitatively correct description of the anomalous relaxation, which is consistent with incipient inhomogeneities. More recently, Venerus (Venerus, 2005; Venerus and Nair, 2006) studied step strain experiments, and concluded that many of the anomalous “type C” responses could be explained by experimental conditions such as wall slip or rheometer compliance; however, a

number of experiments could not be accounted for in this way.

In the last decade or so the advent of high resolution velocimetry has led to a series of exciting experiments, principally by Wang and co-workers, that demonstrate evidence of shear banding in entangled polymers (Tapadia and Wang, 2003, 2004; Boukany and Wang, 2007; Hu *et al.*, 2008a; Ravindranath *et al.*, 2008). Very well-entangled solutions, with entanglement number  $Z \gtrsim 40 - 50$ , display well-defined steady state shear bands (Wang *et al.*, 2006; Hu *et al.*, 2007, 2008a; Ravindranath *et al.*, 2008; Boukany and Wang, 2009b). This occurs in both synthetic polymers, such as polybutadiene (Ravindranath *et al.*, 2008), and DNA (Boukany *et al.*, 2008; Boukany and Wang, 2009a; Hu *et al.*, 2008b; Boukany and Wang, 2009b). Polydisperse systems exhibit smoother, less well-defined (or no) shear banding (Boukany and Wang, 2007), possibly because the many timescales smear out the instability (as suggested by Doi and Edwards (1979) in their original paper).

There have been numerous improvements upon the original DE theory, notably to incorporate convective constraint release (CCR) (Marrucci, 1996; Mead *et al.*, 1998; Milner *et al.*, 2001). CCR can reduce the severity of the DE instability and potentially render the fluid stable (Graham *et al.*, 2003), and DE-CCR models can capture, at least qualitatively, many of the shear banding signatures of these experiments. This was recently shown by Adams and Olmsted (2009b,a) in calculations based on the Rolie-Poly model (Likhtman and Graham, 2003), a simple one-mode differential version of DE theory that incorporates CCR and chain stretch. However, there is no consensus yet as to the correct level of CCR required to describe existing experiments.

In related work, Zhou *et al.* (2008) showed that a non-monotonic constitutive relation based on the “partially extending convective strain” model of Larson (1984) also reproduces many of the features of the recent experiments, including recoil during startup onto the banding plateau, and strain localization immediately after a step strain effected by shearing at a very fast finite shear rate.

Numerous experiments also show inhomogeneous behavior in fluids that do not display steady state shear banding (smaller entanglement number  $Z$ ). Examples include: (1) transient band formation and recoil during startup, which eventually gives way to homogeneous shear flow (Tapadia and Wang, 2006; Hu *et al.*, 2007; Ravindranath *et al.*, 2008; Boukany and Wang, 2009b); (2) extremely sharp shear banding during portions of the cycle during Large Amplitude Oscillatory Shear (LAOS) (Tapadia *et al.*, 2006; Ravindranath and Wang, 2008; Zhou *et al.*, 2010); (3) inhomogeneous response (including negative velocity recoil) after step strain performed at high shear rates (Wang *et al.*, 2006; Ravindranath and Wang, 2007).

At a constitutive level, one cause of steady state shear banding is a non-monotonic steady state constitutive

relation (such as the DE theory with sufficiently weak CCR), which cannot support stable homogeneous steady states for a range of shear rates. However, the same criterion clearly cannot determine the apparent instability to transient banding in fluids that don’t shear band in steady state (*i.e.* that have monotonic flow curves). Evidently these fluids are dynamically unstable, which need not be related to a steady state non-monotonic constitutive relation.

Indeed, pronounced transient shear banding has recently been reported by Divoux *et al.* (2010) in a yield stress fluid with a monotonic steady state constitutive curve, and captured theoretically in shear transformation zone (STZ) theories (Manning *et al.*, 2007, 2009), a modified soft glassy rheology (SGR) model (Moorcroft *et al.*, 2011), a simplified fluidity model (Moorcroft *et al.*, 2011), and a mesoscopic model of plasticity (Jagla, 2010).

Several, possibly related, explanations for the transient banding can be envisioned:

1. The dynamical equations of motion passes through a regime of parameter space, as a function of time, in which the homogeneous instantaneous state is dynamically unstable to small spatial perturbations. Such perturbations will initially grow in time before eventually decaying to a homogeneous steady state. However, if the instability is strong enough the perturbations could grow into a macroscopically observable transient band before decaying. We will perform this linear stability calculation here, and show that this gives an understanding of the transient homogeneities. A similar calculation was done by Fielding and Olmsted (2003) for wormlike micelles undergoing steady state banding.
2. The fluid possesses, at any observation time  $t_m$ , an *instantaneous* constitutive curve  $\sigma_{xy}(\dot{\gamma}, t_m)$ . Such a constitutive curve can be constructed by performing a number of startup evolutions (calculations or experiments) at different shear rates, which then define the loci of stress as a function of shear rate for given observation times  $t_m$  after flow inception. Since most of these points are not in steady state, the resulting curve need not be monotonic even if the shear rate remains homogeneous. Then, one could associate a negative slope  $\partial\sigma_{xy}(\dot{\gamma}, t_m)/\partial\dot{\gamma} < 0$  with transient inhomogeneities. However, this only addresses a subspace of the full parameter space considered by the first scenario above and could thus only serve as a rough guideline. One must also carefully distinguish between theoretical calculations in which a homogeneous shear rate can be specified, and the experimental protocol above, in which the fluid will be expected to become inhomogeneous after the onset of an instability. This procedure was recently suggested by Hayes *et al.* (2010) in experiments using parallel plate rheometry of polymer solutions.

3. For very strong shear rates these viscoelastic fluids respond elastically, like a non-linear solid, and can display a stress overshoot. In this case the mechanism of Marrucci and Grizzuti (1983) might be expected to apply, as follows. For a given imposed shear rate  $\dot{\gamma}$  the stress  $\sigma_{xy}$  is a function of strain  $\gamma = \dot{\gamma}t$ . A solid with a negative gradient  $\partial\sigma_{xy}/\partial\gamma < 0$  has an effective negative differential shear modulus, which leads to elastic instability. This would imply that, for shear rates large enough to remain in the elastic regime, a stress overshoot upon startup could signify an instability to inhomogeneous flows. [Note that the MG argument is strictly for an ideal step strain, rather than a strain incurred during a fast but finite shear rate]. Sui and McKenna (2007) pointed this out in their recent visualization study of the same materials studied by Tapadia and Wang (2006). This scenario is suggested by data showing correlations between transient banding and stress overshoots (*e.g.* the Figures 3 and 4 of Boukany *et al.* (2008)), and by calculations that show similar correlations (*e.g.* Figure 3 of Adams and Olmsted (2009b), for both monotonic and non-monotonic constitutive curves).

In this paper we explore these different scenarios, and thus the detailed conditions necessary for transient inhomogeneities, using the diffusive Rolie-Poly (DRP, or RP) model as an example (Likhtman and Graham, 2003). We calculate its instantaneous linear stability for parameters ranging from monotonic to non-monotonic constitutive behavior. We show that even fluids with monotonic constitutive curves, which have stable homogeneous steady states, can have periods of instability during startup flow. For some parameters, strong linear instability is shown to lead to transient banding and negative velocity recoil in the full non-linear dynamics.

Since instabilities require an initial perturbation to manifest in eventual non-linear growth, we will study two natural perturbations: (1) stress gradients, as found in typical circular rheometric devices (cone and plate or cylindrical Couette), and (2) non-uniform (noisy) initial conditions. We find a strong link between transient inhomogeneities, stress overshoots, and an instantaneous non-monotonic constitutive curve, but we leave further detailed analysis of this for future work.

We compare our calculations with recent experiments on transient data after startup to steady state. For conciseness, we do not study the inhomogeneous response to a step strain, though our results give a quantitative method for understanding this behavior as well.

## II. THE DIFFUSIVE ROLIE-POLY MODEL

### A. Momentum Balance

Newton's force balance for the fluid is given by

$$\rho \frac{D\mathbf{v}}{Dt} = \nabla \cdot \boldsymbol{\sigma} \quad (1)$$

where  $\rho$  is the density,  $\boldsymbol{\sigma}$  is the total stress, and  $D/Dt$  is the material derivative. We will use the full equation set (at finite but small Reynolds number) for the linear stability analysis in section IV A, but take the zero Reynolds number (creeping flow) limit for calculating the full spatially resolved non-linear dynamics in section IV B. In the latter case the equation of motion reduces to

$$\nabla \cdot \boldsymbol{\sigma} = 0. \quad (2)$$

For the experimental cases of interest we expect very small Reynolds number  $\text{Re} \ll 10^{-3}$ .

### B. Stress

The total stress  $\boldsymbol{\sigma}$  in a polymer solution is assumed to comprise an elastic stress carried by the backbone of the polymers (due to their stretching and orientation), and viscous drag against solvent and other polymers. In polymer melts the viscous stress can usually be safely neglected, particularly for weak flows (Doi and Edwards, 1989). However, for strong flows, where DE theory predicts a strongly decreasing polymeric stress due to tube alignment, it is necessary to incorporate additional viscous stresses from the faster degrees of freedom. This includes the Newtonian solvent viscosity of solutions, as well as fast Rouse modes and interpolymer viscous friction neglected in the simplest tube models. In addition to this crucial argument, a second contribution to the total stress is physically necessary to describe steady state shear banding in planar Couette flow, in which the shear rate is inhomogeneous but the total stress must be homogeneous.

Hence, we represent the total stress as two separate components: fast Newtonian (or solvent) degrees of freedom, and the slow viscoelastic stress  $G\mathbf{W}$ :

$$\boldsymbol{\sigma} = -p\mathbf{I} + 2\eta\mathbf{D} + G\mathbf{W}, \quad (3)$$

where  $\mathbf{I}$  is the identity tensor,  $\mathbf{D} = \frac{1}{2} [\nabla\mathbf{v} + (\nabla\mathbf{v})^T]$ ,  $\mathbf{v}$  is the velocity field,  $p$  is the isotropic pressure determined by incompressibility ( $\nabla \cdot \mathbf{v} = 0$ ),  $\eta$  is the solvent viscosity, and  $G$  is the plateau modulus. In this representation the quantity  $\mathbf{W}$  is the polymer, or viscoelastic, strain, whose stress  $G\mathbf{W}$  is parametrized by the elastic modulus  $G$ . Together with a DE-like constitutive relation for  $\mathbf{W}$ , Eq. (3) can yield either a monotonic or a non-monotonic constitutive relation, with a Newtonian high shear rate branch.

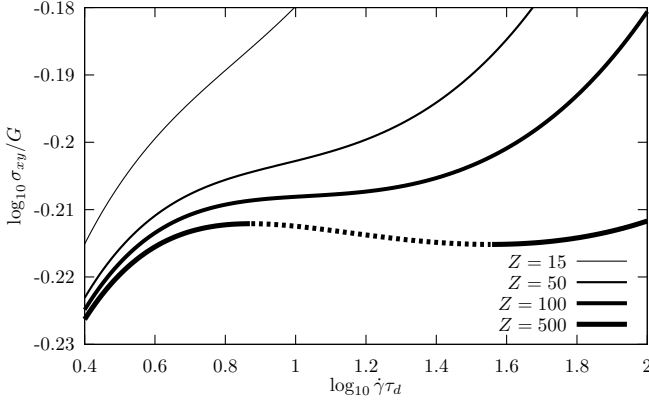


FIG. 1. Constitutive curves for the Rolie-Poly model, showing monotonic and non-monotonic behavior as a function of entanglement number  $Z$ ; for  $\beta = 0.65$  and  $\epsilon = 10^{-5}$ .

### C. Rolie-Poly Model

There are many possible constitutive models for the polymeric strain  $\mathbf{W}$  (Islam and Archer, 2001; Mead *et al.*, 1998), but here we will use the diffusive Rolie-Poly (DRP) model of Likhtman and Graham (2003). This is a single mode approximation to the GLAMM model (Likhtman *et al.*, 2000; Milner *et al.*, 2001; Graham *et al.*, 2003), and includes convective constraint release (CCR), reptation of the polymers within their tubes, and the stretching of the polymer chains. The constitutive equation for the deviatoric part of the viscoelastic strain  $\mathbf{W}$  is

$$(\partial_t + \mathbf{v} \cdot \nabla) \mathbf{W} - (\nabla \mathbf{v})^T \cdot \mathbf{W} - \mathbf{W} \cdot (\nabla \mathbf{v}) + \frac{1}{\tau_d} \mathbf{W} = 2\mathcal{D} - \frac{2}{\tau_R} (1 - A) (\mathbf{I} + \mathbf{W} + \beta A^{-2\delta} \mathbf{W}) + \mathcal{D} \nabla^2 \mathbf{W}, \quad (4)$$

where

$$A(\mathbf{W}) = (1 + \text{tr} \mathbf{W} / 3)^{-1/2}, \quad (5)$$

$\tau_d$  is the disengagement time,  $\tau_R$  is the Rouse time, and  $\beta$  parametrizes the efficiency and rate of CCR. The ratio of disengagement to Rouse times defines the entanglement number (Larson *et al.*, 2003)

$$Z = \frac{1}{3} \frac{\tau_d}{\tau_R}. \quad (6)$$

We have added ‘diffusion’ (the term with coefficient  $\mathcal{D}$ ) to the original Rolie-Poly model, to be able to resolve spatial structure during shear banding (Lu *et al.*, 2000; Olmsted *et al.*, 2000). The width of the interface between shear bands is proportional to  $\sqrt{\mathcal{D}}$ .

The RP model does not reproduce all the same constitutive behavior features of the full GLAMM constitutive model (notably, the high shear rate behaviors of the normal and shear stresses differ), primarily because only a

single mode of the GLAMM model has been kept in obtaining the RP model. However, it is simple enough to perform spatially resolved simulations in the presence of the added diffusive term. The additional solvent stress,  $2\eta \mathbf{D}$  in Eq. (3), was not included in the original formulation, which was focused on melts and not on shear banding behavior.

### D. Choice of Parameters

Likhtman and Graham (2003) chose  $\beta = 0.5$  and  $\delta = -1/2$ , which optimized the comparison with transient and steady state measurements within the assumption of homogeneous flows. The negative value for  $\delta$  ensures that CCR decreases for large stretch, due to the increased number of effective entanglements. The high shear rate scaling of the total shear stress  $\sigma_{xy}$  in the RP model is

$$\frac{\sigma_{xy}}{G} = \begin{cases} \left[ \frac{1}{(6Z+1)^2} + \epsilon \right] \dot{\gamma} \tau_d & (\delta \leq 0) \\ \left( \frac{3^\delta \dot{\gamma} \tau_d}{6Z\beta 2^\delta} \right)^{\frac{1}{1+2\delta}} + \epsilon \dot{\gamma} \tau_d & (\delta > 0), \end{cases} \quad (7)$$

where

$$\epsilon = \frac{\eta}{G\tau_d} \quad (8)$$

is the ratio between the solvent viscosity and that of the quiescent entangled solution. Typical experimental values for the parameters are  $\epsilon \sim 10^{-3} - 10^{-5}$  and  $Z \sim 15 - 200$  (Adams and Olmsted, 2009b; Tapadia and Wang, 2006).

As can be seen above, the choice  $\delta = -1/2$  leads to a Newtonian high shear rate branch, with slope dominated by the entanglement contribution for typical values of  $\epsilon$  and  $Z$ . This is inconsistent with the experiments of Tapadia and Wang (2003), which suggest a scaling  $\sigma_{xy} \sim \dot{\gamma}^{1/2}$  at high shear rate. This scaling can be produced by choosing  $\delta = 1/2$  (Eq. 7), which leads to

$$\frac{\sigma_{xy}}{G} = \left( \frac{3^{1/2} \dot{\gamma} \tau_d}{6Z\beta 2^{1/2}} \right)^{\frac{1}{2}} + \epsilon \dot{\gamma} \tau_d. \quad (9)$$

This has an intermediate scaling  $\sigma_{xy} \sim \dot{\gamma}^{1/2}$ , before giving way at the highest shear rates to Newtonian behavior. However, this choice does a poorer job at the validation tests carried out by Likhtman and Graham (2003) and has the incorrect physical interpretation of the effect of stretch on CCR (as noted above), and for these reasons we use  $\delta = -1/2$  here.

The Newtonian power law in the high shear rate branch, which applies for our choice  $\delta = -1/2$ , produces a relatively narrow stress plateau. This is one of the unsatisfactory approximations to the GLAMM model that may explain why such a large  $Z$  value (compared to experiments) is required for the RP model to exhibit velocity recoil and transient banding. This is an obvious and important direction for future work.



### E. Constitutive Relations

The RP model readily admits non-monotonic constitutive curves that can display shear banding, depending on the values of the CCR parameter  $\beta$ , the entanglement number  $Z$ , and the solvent viscosity  $\epsilon$ . For smaller  $\epsilon$  and larger  $Z$  there is a wider separation between the high and low shear rate branches, while the CCR parameter controls whether the crossover between the two regimes contains a decreasing stress (smaller  $\beta$  or less active CCR) or is monotonic (larger  $\beta$  or more active CCR). Fig. 1 shows the effect of changing the number of entanglements for fixed solvent viscosity and CCR parameter, while Fig. 2 illustrates the effect of varying the the CCR parameter.

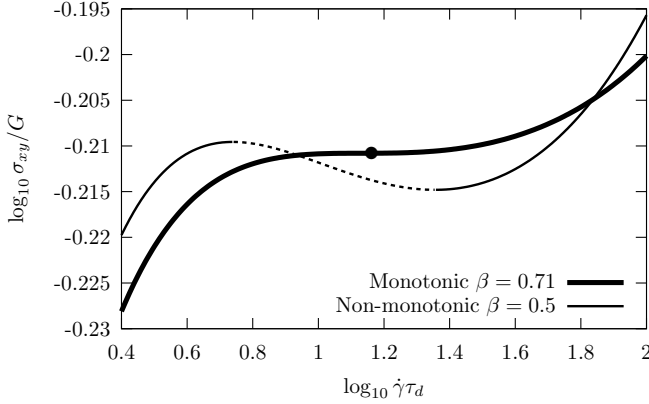


FIG. 2. Monotonic and non-monotonic constitutive curves arising from the Rolie-Poly model obtained by varying the CCR parameter  $\beta$ , for  $\epsilon = 10^{-5}$  and  $Z = 265$ . The marked point at  $\log_{10} \dot{\gamma} \tau_d = 1.138$  ( $\dot{\gamma} \tau_d = 13.74$ ) on the monotonic constitutive curve is studied in detail in Figs. (4,5,6).

The parameters space  $(\beta, \epsilon, Z)$  for the Rolie-Poly model can be divided into regions of monotonic and non-monotonic constitutive curves, illustrated in Fig. 3. Non-monotonic curves occur for small values of  $\epsilon$ , small values of  $\beta$ , and large  $Z$ .

In what follows we will illustrate the transient banding-like behavior associated with monotonic constitutive relations. We will study the dynamics of startup to a shear rate that is on the plateau region, and which eventually yields a non-banded homogeneous steady state. Transient banding behavior develops under these conditions, and we will explain this with the help of linear stability analysis. We primarily use the parameters  $(\beta, \epsilon, Z) = (0.71, 10^{-5}, 265)$ , corresponding to the thick line in Fig. 2. Unfortunately,  $Z = 265$  is much higher than the values  $Z \gtrsim 40 - 50$  needed to see shear banding experimentally. We believe that this is because the Rolie-Poly model, as discussed above, only roughly approximates the full microscopic theory of the GLAMM model, which is itself an approximation; hence we caution the reader against over-interpreting the values of these parameters. We will return later to briefly discuss this point.

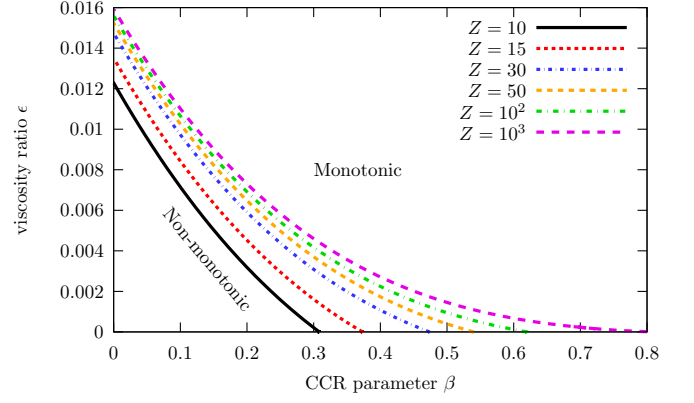


FIG. 3. Lines separating monotonic (upper right) from non-monotonic (lower left) constitutive behavior as a function of the viscosity ratio  $\epsilon$  and CCR parameter  $\beta$ , for different entanglement numbers  $Z$ .

### III. DYNAMICS AND BOUNDARY CONDITIONS

#### A. Flow geometry

We consider Couette flow between concentric cylinders of inner (outer) radii  $R_1$  ( $R_2$ ), in cylindrical coordinates with flow varying only in the radial direction,  $\mathbf{v} = v(r)\hat{\theta}$ . Using this description the tangential and radial components of the force balance conditions are respectively given by

$$\rho \dot{v} = \frac{1}{r^2} \partial_r (r^2 \sigma_{r\theta}) \quad (10)$$

$$-\rho \frac{v^2}{r} = \partial_r \sigma_{rr} + \frac{\sigma_{rr} - \sigma_{\theta\theta}}{r}, \quad (11)$$

and the components of the polymer strain  $\mathbf{W}$  obey

$$\mathcal{L}W_{\theta\theta} - 2W_{r\theta}\dot{\gamma} = -\frac{2}{\tau_R}(1-A) + \frac{2\mathcal{D}}{r^2}(W_{rr} - W_{\theta\theta}) \quad (12a)$$

$$\mathcal{L}W_{rr} = -\frac{2}{\tau_R}(1-A) + \frac{2\mathcal{D}}{r^2}(W_{\theta\theta} - W_{rr}) \quad (12b)$$

$$\mathcal{L}W_{zz} = -\frac{2}{\tau_R}(1-A) \quad (12c)$$

$$\mathcal{L}W_{r\theta} - W_{rr}\dot{\gamma} = \dot{\gamma} - \frac{4\mathcal{D}}{r^2}W_{r\theta}, \quad (12d)$$

where  $\dot{\gamma} = r\partial_r(\frac{v}{r})$  is the local shear rate and we have defined the nonlinear operator

$$\mathcal{L} = \partial_t - \frac{\mathcal{D}}{r} \partial_r r \partial_r + \frac{1}{\tau_d} + \frac{2}{\tau_R} [1 - A(\mathbf{W})] [1 + \beta A(\mathbf{W})]. \quad (13)$$

The constitutive equations can be simplified by parametrizing the spatial coordinate by

$$r = R_1 e^{qy}, \quad (14)$$

where

$$q = \ln \frac{R_2}{R_1} \quad (15)$$

is a measure of the curvature of the measurement device, and the dimensionless coordinate  $y \in [0, 1]$  spans the width of the gap  $L = R_2 - R_1$  (Greco and Ball, 1997).

The relative stress difference between the two cylinders is given by

$$\frac{\sigma_{r\theta}(R_1) - \sigma_{r\theta}(R_2)}{\sigma_{r\theta}(R_2)} = 1 - e^{-2q}. \quad (16)$$

A Couette cell with radii  $R_1 = 2$  cm,  $R_2 = 2.1$  cm has  $q = 0.049$ . In a cone and plate device the stress varies as (Larson, 1999)

$$\sigma_{\theta\phi} = \frac{\sigma_{\theta\phi}(\theta = \pi/2)}{\sin^2 \theta}, \quad (17)$$

where  $\theta$  is measured with respect to the normal vector to the plate. Hence the stress variation between the cone and plate is

$$\frac{\sigma_{\theta\phi}(\alpha) - \sigma_{\theta\phi}(0)}{\sigma_{\theta\phi}(0)} = \tan^2 \alpha, \quad (18)$$

where  $\alpha$  is the cone angle. For cone angles  $\alpha = \pi/2 - \theta \equiv 4^\circ$  and  $1^\circ$  the stress difference is roughly equivalent to the values  $q = 2 \times 10^{-3}$  and  $q = 2 \times 10^{-4}$ , respectively (Adams *et al.*, 2008). In what follows we will sometimes compare the stress variation of a cone and plate geometry to the equivalent stress variation of a Couette cell with a particular geometric parameter  $q$ : however, we do not perform calculations for the cone and plate geometry.

We change to dimensionless quantities, labelled by  $\tilde{\cdot}$ , by measuring time in units of the disengagement time  $\tau_d$  and stress in units of the plateau modulus  $G$ , so that the total shear stress is expressed as

$$\tilde{\sigma}_{r\theta} = W_{r\theta} + \epsilon \tilde{\gamma}, \quad (19)$$

where  $\tilde{\gamma} = \dot{\gamma} \tau_d$  and  $\tilde{\sigma}_{r\theta} = \sigma_{r\theta}/G$ . We define a dimensionless diffusion constant

$$D \equiv \frac{\mathcal{D} \tau_d}{(q R_1)^2}. \quad (20)$$

Note that the inner radius  $R_1$  can be written in terms of the gap  $L$  between cylinders as

$$R_1 = \frac{L}{e^q - 1}, \quad (21)$$

so that  $q R_1$  depends only weakly on  $q$  for small  $q$ . Below we will use  $D$  and  $q$  as independent parameters. Because we consider small  $q \lesssim 10^{-2}$ , the dependence of  $D$  on  $q$  is negligible. Hence, by fixing  $D$  and varying  $q$  we can separate the effects of the total stress gradient, as parametrized by  $q$ , from the effects of the finite width  $\sqrt{D}$  of the interface.

In this representation the constitutive equation becomes

$$\tilde{\mathcal{L}}X = -6(1-A)Z + 2S\tilde{\gamma} + 2De^{-2qy}(Y-X) \quad (22a)$$

$$\tilde{\mathcal{L}}Y = -6(1-A)Z - 2De^{-2qy}(Y-X) \quad (22b)$$

$$\tilde{\mathcal{L}}W = -6(1-A)Z \quad (22c)$$

$$\tilde{\mathcal{L}}S = (1+Y)\tilde{\gamma} - 4De^{-2qy}S, \quad (22d)$$

where  $X = W_{\theta\theta}$ ,  $Y = W_{rr}$ ,  $W = W_{zz}$ , and  $S = W_{r\theta}$ , and  $Z$  is the entanglement number given by Eq. (6). The nonlinear operator is thus

$$\tilde{\mathcal{L}} = \partial_{\tilde{t}} - De^{-2qy}\partial_y^2 + 1 + 6Z(1-A)(1+\beta A), \quad (23)$$

and the momentum balance equations become

$$\tilde{\rho}\tilde{v} = e^{-3qy}\partial_y(e^{2qy}\tilde{\sigma}_{r\theta}) \quad (24)$$

$$-\tilde{\rho}\tilde{v} = \frac{1}{q}\partial_y\tilde{\sigma}_{rr} + (\tilde{\sigma}_{rr} - \tilde{\sigma}_{\theta\theta}). \quad (25)$$

where  $\tilde{\rho} = \frac{\rho L^2}{G \tau_d^2}$ . The dimensionless velocity is scaled by  $\tau_d$  and a length  $R_1(e^q - 1)$  that becomes the plate separation  $R_2 - R_1 = L$  in the  $q \rightarrow 0$  limit.

Planar Couette flow obtains in the limit  $q \rightarrow 0$ , with the correspondences  $\hat{\mathbf{r}} \rightarrow -\hat{\mathbf{y}}$ ,  $\hat{\boldsymbol{\theta}} \rightarrow \hat{\mathbf{x}}$ ,  $q \rightarrow 0$  and  $q R_1 \rightarrow L$ , and the force balance conditions become  $\tilde{\rho}\tilde{v} = \partial_y(\tilde{\sigma}_{yx})$  and  $\partial_y\tilde{\sigma}_{yy} = 0$ .

## B. Boundary Conditions

An imposed cylinder rotation rate  $V/R_1$  can be expressed in terms of the integral of the shear rate across the gap by

$$-\frac{V}{R_1} = \int_{R_1}^{R_2} \dot{\gamma} \frac{dr}{r} = \int_0^1 \dot{\gamma} q dy \quad (26)$$

The average applied shear rate is

$$\langle \dot{\gamma} \rangle \equiv \frac{1}{q} \int_{R_1}^{R_2} \dot{\gamma} \frac{dr}{r} = \int_0^1 \dot{\gamma} dy. \quad (27)$$

which reduces to  $-V_1/L$  in the planar limit. We assume that there is no slip at the walls, despite the fact that wall slip can be important experimentally (Wang, 1999; Boukany *et al.*, 2006; Boukany and Wang, 2009a).

The presence of spatial gradients in the form of the ‘diffusion’ term necessitates a boundary condition on the viscoelastic strain  $\mathbf{W}$ . Although it is possible to incorporate sophisticated wall constitutive models (Black and Graham, 1996) or complex boundary conditions (Rossi *et al.*, 2006; Adams *et al.*, 2008), we will use the simplest Neumann boundary conditions for the polymer strain,

$$(\hat{\mathbf{n}} \cdot \nabla) \mathbf{W} = 0 \text{ for } y = 0, 1; \quad (28)$$

here  $\hat{\mathbf{n}}$  is the normal to the boundary.

## IV. CALCULATIONAL METHODS

### A. Linear Stability Analysis

We first analyze the linear stability of Eqs. (22) above, in the planar limit ( $q \rightarrow 0$ ), which should be a good approximation of the behavior of typical systems for which  $q \simeq 0.0001 - 0.05$ . We follow the stability analysis performed for the Johnson-Segalman model by Fielding and Olmsted (2003), who showed that fluids with non-monotonic constitutive curves are unstable during startup at fixed shear rate to spatial perturbations, which ultimately develop into shear bands. We will apply this to monotonic constitutive curves such as shown in Fig. 2.

The equations of motion are first solved for a homogeneous time-dependent solution, which we refer to as the homogeneous base state. We study the time dependence of inhomogeneous perturbations about this homogeneous base state. If these perturbations grow in time then the homogeneous time-dependent base state is unstable to inhomogeneous states, which we refer to as transient banding. Hence, we linearize the Navier-Stokes equation and the Rolie-Poly constitutive equations around a uniform time dependent base state (denoted by subscripts 0),  $X = X_0 + \delta X$ ,  $Y = Y_0 + \delta Y$ ,  $W = W_0 + \delta W$ ,  $S = S_0 + \delta S$  and  $\tilde{\gamma} = \tilde{\gamma}_0 + \delta \tilde{\gamma}$ . The linearized Navier-Stokes equation

(Eq. 11) is

$$\tilde{\rho} \partial_t \delta \tilde{\gamma} = \partial_y^2 \delta S + \epsilon \partial_y^2 \delta \tilde{\gamma}, \quad (29)$$

where  $\tilde{\gamma} = \partial_y \tilde{v}$ . Note that  $\tilde{\rho}$  is exceedingly small ( $\tilde{\rho} \sim 10^{-9}$ ) for the experiments of interest (Tapadia *et al.*, 2006), and justifies the creeping flow limit in section IV B. However, we keep this term in the linear stability analysis for completeness; leaving it out has no discernible effect for physically realistic values.

We now consider spatial fluctuations in all quantities,

$$\delta \mathbf{u}(y) = \sum_k \delta \mathbf{u}_k e^{iky}, \quad (30)$$

$$\mathbf{u} \equiv (X, Y, W, S, \tilde{\gamma}), \quad (31)$$

where  $\delta \mathbf{u}_k = \delta \mathbf{u}_{-k}^*$  because the function  $\delta \mathbf{u}(y)$  is real. The boundary conditions of Eq. (26) on the shear rate  $\tilde{\gamma}$  quantize the values of the wavenumber,  $k = n\pi$  ( $n = 1, 2, 3, \dots$ ), to keep the average shear rate across the gap fixed to the imposed value.

Linearizing Eqs. (22, 29) about the homogeneous instantaneous state produces a matrix equation of the form

$$\partial_t \delta \mathbf{u}_k = \mathbf{M}(k, t) \cdot \delta \mathbf{u}_k, \quad (32)$$

where the stability matrix is given by

$$\mathbf{M} = \begin{bmatrix} \Pi - ZA^3(1 + \Gamma X) & -A^3Z(1 + \Gamma X) & -A^3Z(1 + \Gamma X) & 2\tilde{\gamma} & 2S \\ -A^3Z(1 + \Gamma Y) & \Pi - ZA^3(1 + \Gamma Y) & -A^3Z(1 + \Gamma Y) & 0 & 0 \\ -A^3\Gamma ZW & -A^3Z(1 + \Gamma W) & \Pi - ZA^3(1 + \Gamma W) & 0 & 0 \\ -A^3\Gamma ZS & -A^3\Gamma WS + \tilde{\gamma} & -A^3\Gamma ZS & \Pi & 1 + Y \\ 0 & 0 & 0 & -\frac{k^2}{\tilde{\rho}} & -\frac{k^2\epsilon}{\tilde{\rho}} \end{bmatrix}, \quad (33)$$

with

$$\Pi = -1 - Dk^2 - 6Z(1 - A)(1 + A\beta) \quad (34)$$

$$\Gamma = 1 - \beta + 2A\beta. \quad (35)$$

The matrix depends on the values of the shear rate and polymer strain at a time  $t$ , determined according to homogeneous evolution of the dynamics. A linear disturbance  $\delta \mathbf{u}_k$  will grow exponentially in time if an eigenvalue  $\omega_\alpha$  of  $\mathbf{M}$  has positive real part (Fielding and Olmsted, 2003). We define  $\omega_{\max}$  as the eigenvalue with the largest real part  $\Re(\omega_\alpha)$ . To analyze the stability of the transients with respect to spatial fluctuations we calculate the evolution of the eigenvalues of  $\mathbf{M}$  as a function of time  $t$ , using the homogeneous solution  $\mathbf{W}(t)$  for the un-

perturbed state at a given time.

A useful measure of the duration and severity of instability is the total ‘weight’  $\Omega_{\max}$  of the instability, obtained by integrating the real part of  $\omega_{\max}$  over all time during which it is positive:

$$\Omega_{\max} = \int_0^\infty \text{Max}(0, \Re(\omega_{\max})) dt. \quad (36)$$

For larger weights  $\Omega_{\max}$  we expect the fluid to enter the non-linear regime and develop a transient shear band, after which stable homogeneous flow is restored in steady state (for monotonic constitutive curves). This is verified by the full non-linear calculation, to which we now turn.

## B. Spatially resolved Rolie-Poly model

We have thus far addressed the evolution of the homogeneous model, and the linear (in)stability of this evolution to inhomogeneous states. To compute the full inhomogeneous non-linear dynamics we solve the creeping flow equation, Eq. (2), and the DRP constitutive equations, Eqs. (22), with a constrained shear rate, Eq. (26) and the boundary conditions, Eq. (28). This leads to a set of coupled second order partial differential equations. A uniform spatial grid of 500 points was used to discretize the equations, and a semi-implicit Crank-Nicolson scheme was used to effect the time evolution. We have checked convergence with respect to timestep and spatial mesh. Typical dimensionless time steps were  $10^{-5}$ , with dimensionless spatial meshes of  $2 \times 10^{-3}$ ; and a dimensionless diffusion constant  $D = 4 \times 10^{-4}$  was used, corresponding to an effective dimensionless diffusion length  $2 \times 10^{-2}$ .

The shear rate constraint of Eq. (26) was implemented by integrating Eq. (24) in the zero Reynolds number limit to obtain

$$Te^{-2qy} = \tilde{\sigma}_{r\theta} = W_{r\theta} + \epsilon \tilde{\gamma}, \quad (37a)$$

$$T = \frac{2q}{1 - e^{-2q}} [\langle W_{r\theta} \rangle + \epsilon \langle \tilde{\gamma} \rangle], \quad (37b)$$

where  $T$  is the torque per unit length applied to the inner cylinder. Eqs. (37) were then used to eliminate the local shear rate  $\tilde{\gamma}(y)$  in Eqs. (22) in terms of the torque and the local value of the polymer shear strain  $W_{r\theta}(y)$ :

$$\tilde{\gamma}(y) = \frac{1}{\epsilon} [Te^{-2qy} - W_{r\theta}(y)]. \quad (38)$$

The torque per unit length  $T$  can be computed at any instant in time from the full inhomogeneous profile in terms of the spatial averages of  $W_{r\theta}$  and  $\tilde{\gamma}$ , as defined in Eq. (37b).

There are several possible measures of the degree of inhomogeneity in the spatially resolved flow profile. At any instant we define the shear rate drop

$$\Delta = \frac{|\dot{\gamma}_{\max} - \dot{\gamma}_{\min}|}{\langle \dot{\gamma} \rangle}, \quad (39)$$

where  $\dot{\gamma}_{\max}$  (resp.  $\dot{\gamma}_{\min}$ ) is the maximum (resp. minimum) of the measured shear rate profile, which should be easily accessible from experimental data. Other measures could include the variance of the shear rate values across the sample cell, or the maximum local gradient of the shear rate. Since all of these give an equivalent qualitative indication of the development of inhomogeneities during flow, we choose this simple measure.

## V. RESULTS: INSTABILITY AND TRANSIENTS

In this section we study the linear (in)stability of homogeneous startup, and compare this with the non-

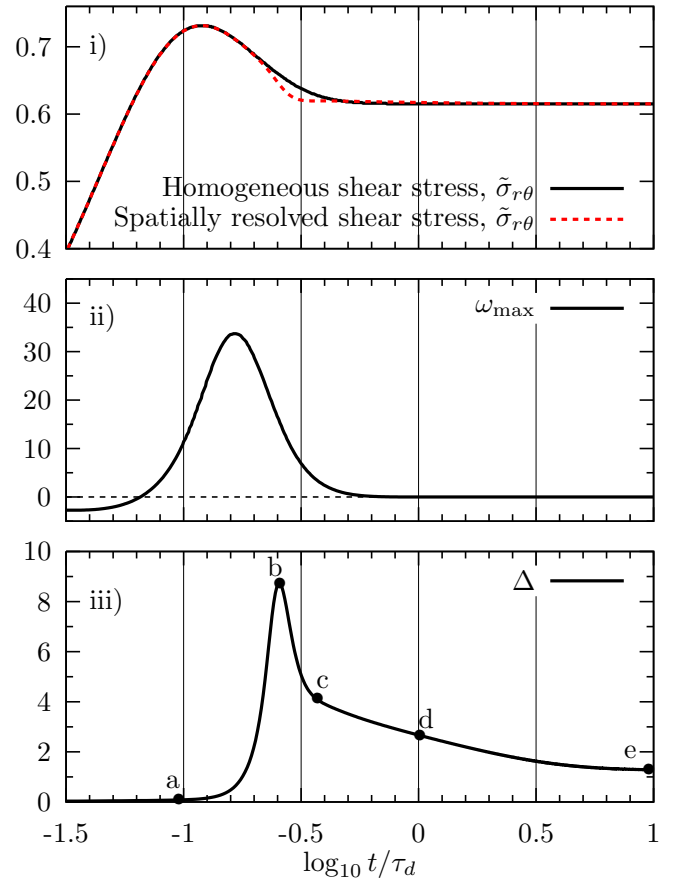


FIG. 4. Evolution of various quantities as a function of time during shear rate startup for parameters  $(\beta, \epsilon, Z) = (0.71, 10^{-5}, 265)$ , for  $q = 10^{-3}$  and applied average shear rate  $\dot{\gamma}\tau_d = 13.74$  ( $\log_{10} \dot{\gamma}\tau_d = 1.138$ ) (the marked point on the monotonic constitutive curve in Fig. 2). (i) Dimensionless total shear stress calculated based on homogeneous flow (solid) or allowing inhomogeneous transients (dashed); (ii) real part of the largest unstable eigenvalue  $\omega_{\max}$ ; (iii) shear rate drop  $\Delta$  (as defined in Eq. 39), as a measure of spatial inhomogeneity showing significant transients during startup. The times a, b, c, d, e are shown as velocity profiles in Fig. 5.

linear spatially-resolved calculations in which the transient shear bands are allowed to form naturally. Here we consider an initial state at rest with no ‘noise’, in a weakly curved geometry  $q = 10^{-3}$ . In Sec. VI we will study the effects of different magnitudes of spatial noise and curvature.

We study model parameter values  $(\beta, \epsilon, Z) = (0.71, 10^{-5}, 265)$ , corresponding to the solid constitutive curve in Fig. 2, for an imposed shear rate  $\dot{\gamma}\tau_d = 13.74$  (the marked point at  $\log_{10} \dot{\gamma}\tau_d = 1.138$ ) and with shear stress gradient parametrized by  $q = 10^{-3}$ . During startup the shear stress overshoots, before settling down to steady state on a time of order  $\tau_d$ . Fig. 4 compares a calculation in which the shear rate remains homogeneous (solid line) with a spatially-resolved calculation that allows for inhomogeneities (dashed line), showing that



the stress decays more rapidly in the spatially-resolved model. The largest unstable eigenvalue, from the linear stability analysis, becomes positive for  $\log_{10}(t/\tau_d) \gtrsim -1.2$ , and reaches a maximum shortly after the stress overshoot. At late times it decays to a slightly negative value, controlled by the very shallow slope of the steady state constitutive curve.

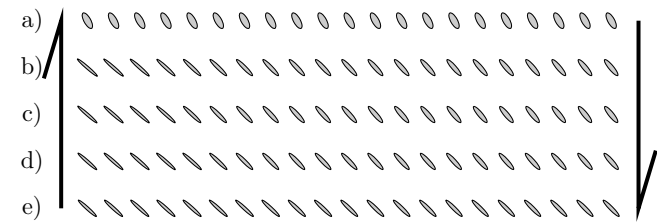
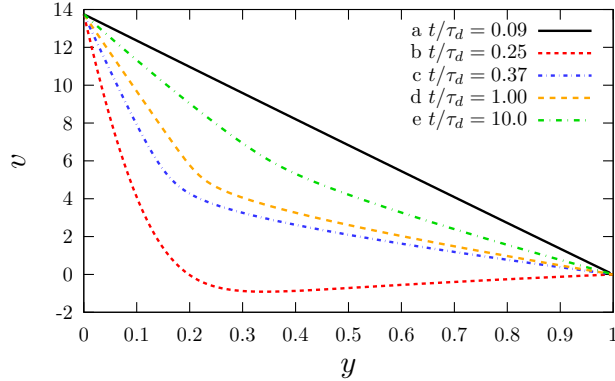


FIG. 5. Velocity profiles during startup flow for the parameters of the marked point  $\log_{10} \dot{\gamma} \tau_d = 1.138$  ( $\dot{\gamma} \tau_d = 13.74$ ) on the monotonic constitutive curve in Fig. 2:  $(\beta, \epsilon, Z) = (0.71, 10^{-5}, 265)$ , for  $q = 10^{-3}$ . The corresponding ellipsoids indicating the components of the  $W_{rr}$ ,  $W_{\theta\theta}$  and  $W_{r\theta}$  components of the polymer strain are shown below. At time  $t = 0.25\tau_d$ , which is shortly after the stress overshoot, both negative recoil velocities and transient shear banding occur. The times labeled a, b, c, d, e are the points labeled on  $\Delta(t)$  in Fig. 4.

Associated with this positive eigenvalue is a pronounced inhomogeneous transient during startup, as evidenced by the shear rate drop  $\Delta$  in Fig. 4 and the velocity profiles in Fig. 5. The most significant heterogeneity comes shortly after the eigenvalue has reached its maximum, after the instability has had sufficient time to develop non-linear consequences. Fig. 5 shows that this maximum (at time  $t = 0.25\tau_d$ , labeled b) corresponds to a dramatic transient banding profile, in which the velocity field has recoiled and become negative at the outer part of the cell (closer to  $y = 1$ ), where the total stress is slightly lower. The strong transient bands decay after a few  $\tau_d$  until the steady state profile is reached. In this case, the stress gradient corresponding to  $q = 10^{-3}$  is enough to induce significant heterogeneity even in steady state (Adams and Olmsted, 2009b) (we will return to the role of the stress gradient in Sec. VI). Fig. 5 also shows the degree of polymer deformation (strain) during the recoil. The polymer strain tensor becomes well-ordered, at

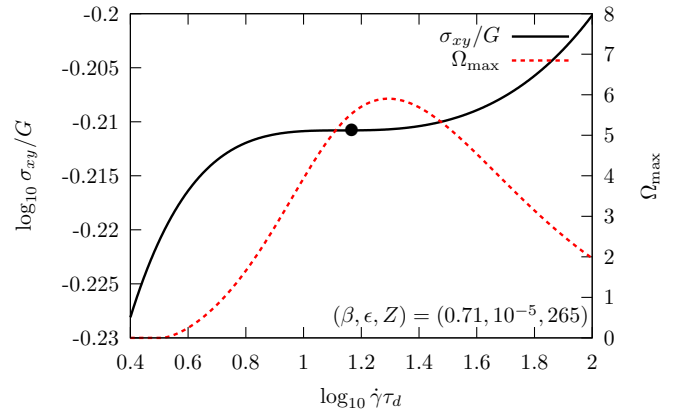


FIG. 6. The weight  $\Omega_{\max}$  of the instability (magnitude of the integral of the most unstable eigenvalue) and the monotonic constitutive curve  $\sigma_{xy}(\dot{\gamma})$  (solid line) from Fig. 2. For  $(\beta, \epsilon, Z) = (0.71, 10^{-5}, 265)$ , for  $q = 10^{-3}$ .

an angle of approximately  $45^\circ$  with respect to the flow direction, when the transient develops (b). Interestingly, it remains ordered and changes only weakly until steady state is reached; moreover, the spatial gradient only introduces a relatively small gradient in the molecular order and orientation. Hence, the transient inhomogeneity would be difficult to observe using a molecular probe such as birefringence or neutron scattering, as compared to explicit measurements of velocity profiles.

Having explored the response to a single shear rate startup protocol, we now study the strength of the instability for different shear rates. Fig. 6 shows the weight  $\Omega_{\max}$  of the instability (integrated unstable eigenvalue) for all applied shear rates for this parameter set. The largest weight occurs near the flattest part of the stress plateau, and indeed we find the clearest transient banding in this region. A detailed study (not shown here) reveals that the weight  $\Omega_{\max}$  is larger for large  $Z$ , small  $\epsilon$  and larger  $\beta$ ; *i.e.* parameters for which the two flow branches are more widely separated and the constitutive curve has a shallower slope. The larger value of  $\beta$  produces a flatter, longer stress plateau.

In summary, transient banding is initiated by a linear instability that begins during startup, and becomes largest shortly after the stress overshoot. If this instability has enough time and strength to grow, as parametrized by the weight  $\Omega_{\max}$ , then transient banding and even recoil can appear before the eventual steady state is reached. The steady state is not banded, but weakly inhomogeneous as specified by the stress gradient across the rheometer.

## VI. THE ROLE OF PERTURBATIONS IN TRANSIENT BANDING

We have seen thus far that inhomogeneous flow, or equivalently transient shear banding, is correlated with

the most unstable eigenvalue governing fluctuations away from a homogeneous state at a given instant in time. We now study the spatial perturbations needed to trigger the instability, by evolving the non-linear inhomogeneous equations of motion. There are several sources of spatial inhomogeneity that could serve this purpose: curved rheometer devices (cone and plate or cylindrical Couette geometries) possess a spatial inhomogeneity in the shear stress; thermal or instrument noise is presumably always present; thermal gradients across the cell may persist; and there may be inhomogeneous initial conditions due to very slow relaxation after sample loading. Here we will study (i) the consequences of a stress gradient due to curved streamlines and (ii) the role of inhomogeneous initial conditions that may arise due to the other effects just mentioned.

We first consider the effect of random initial conditions in a geometry with no intrinsic stress gradient (i. e. planar Couette flow,  $q = 0$ ). A cosine wave with wavelength  $2L$ , in keeping with the boundary conditions, was set as the initial condition for a given polymer strain component, with the others set to zero. The constitutive equations were then evolved and the velocity profile calculated. This was carried out for a range of different amplitudes  $\Lambda$  of the cosine wave. The different components of the polymer strain have markedly different effects: perturbations in  $W_{yy}$  have the most dramatic effect, because this strain component (along the flow gradient) is advected into the polymer shear strain  $W_{xy}$  (Eq. 22d), which in turn directly contributes to the measured total shear stress. Conversely, perturbations in  $W_{xy}$  are much less important because they are rotated into the velocity direction ( $W_{xx}$ ), which does not contribute to the total shear stress. Fig. 7 shows the effect of an initial condition in  $W_{yy}$ . For small enough initial noise there is virtually no transient banding, while substantial initial noise (a few percent of the steady state polymer strain in flow) can lead to strong transient banding and negative velocity recoil. The modulus of entangled polymers is  $G \simeq ck_B T$ , where  $c$  is the concentration of entanglement strands. Reasoning that coherent fluctuations can obtain within a volume of order  $a^3$ , where  $a$  is the tube diameter, Marrucci and Grizzuti (1983) estimated the typical average strain  $\langle \delta W_{\alpha\beta} \rangle$  due to thermal fluctuations in entangled polybutadiene melts to be of order  $\sqrt{1/6.4} \simeq 0.39$ , assuming  $a \simeq 5.8$  nm; this is comparable to the initial condition necessary to induce a transient banding response in our numerical calculation.

The stress overshoot also changes character (Fig. 8): for a larger value of  $\Lambda$  (a stronger perturbation) the stress relaxes more quickly after the overshoot, due to the more rapid development of transient banding. For  $\Lambda = 10^{-2}$  the stress actually *undershoots* the steady state value before increasing and then finally decreasing slowly to the steady state. Similar stress undershoots were reported by Tapadia and Wang (2004) and by Sui and McKenna (2007), for entangled polymer solutions that underwent flow instability; and by Crawley and Graessley (1977) in

much earlier work.

An alternative perturbation is a stress gradient due to, *e.g.*, the curvature of a Couette cell or a non-zero angle in a cone and plate rheometer. This is studied in Fig. 9. As explained earlier we parametrize this by the curvature parameter  $q = \ln R_2/R_1$  (Eq. 15). For  $q > 10^{-3}$ , whose stress gradient is similar to that of very thin gap Couette rheometers or typical cone and plate rheometers, there is substantial transient banding for these parameters; while for  $q = 10^{-5}$  there is essentially no transient banding. [We remind the reader that this calculation was performed for cylindrical Couette flow, and that the comparison with cone and plate flow is based solely on the shear stress gradients in the two geometries.] The stress overshoot also relaxes quicker after the overshoot for a larger stress gradient (larger  $q$ ) (Fig. 10).

An experimental test is thus to observe the change in transient banding as a function of flow geometry and hence  $q$ ; or to systematically pre-shear the material to induce molecular deformation; or otherwise induce or spatially inhomogeneous initial conditions into a sliding plate geometry. Existing experiments show transient banding in both curved and flat geometries; our calculations would be consistent with reproducible transients in a curved geometry, but less reproducible transients in a flat geometry, reflecting the variations of initial and loading conditions.

## VII. DISCUSSION

### A. Parameter Space and Critique of the Rolie-Poly Model

We have explored the behavior of transient banding as a function of the parameters of the DRP model (Fig. 11). A monotonic constitutive curve is more (dynamically) unstable and susceptible to transient banding if it has well separated flow branches, which occurs for greater numbers of entanglements  $Z$ , larger convective constraint release (CCR) efficiency  $\beta$ , and lower solvent viscosity  $\epsilon$ . The larger CCR parameter  $\beta$  may appear paradoxical, since increasing it renders a banding fluid stable. However, one also needs, simultaneously, a smaller viscosity ratio and larger  $Z$ , to render the plateau shallower and wider in the monotonic regime. Although the value of the CCR parameter  $\beta$  is evidently important, we have as yet no way of independently determining it. Likhtman and Graham (2003) used the values of  $\beta = 0, 0.5$  and  $1$  to fit multimode, steady state and transient data respectively. It would be useful to compare a quantitative model such as the DRP model with experimental results on shear banding (transient or steady state) to try and infer the magnitude of the CCR parameter, given knowledge of the other parameters.

Unfortunately the DRP model is still too crude to make this a justifiable exercise. The high shear rate branch is not handled correctly, since Newtonian behavior is not observed experimentally at the highest shear

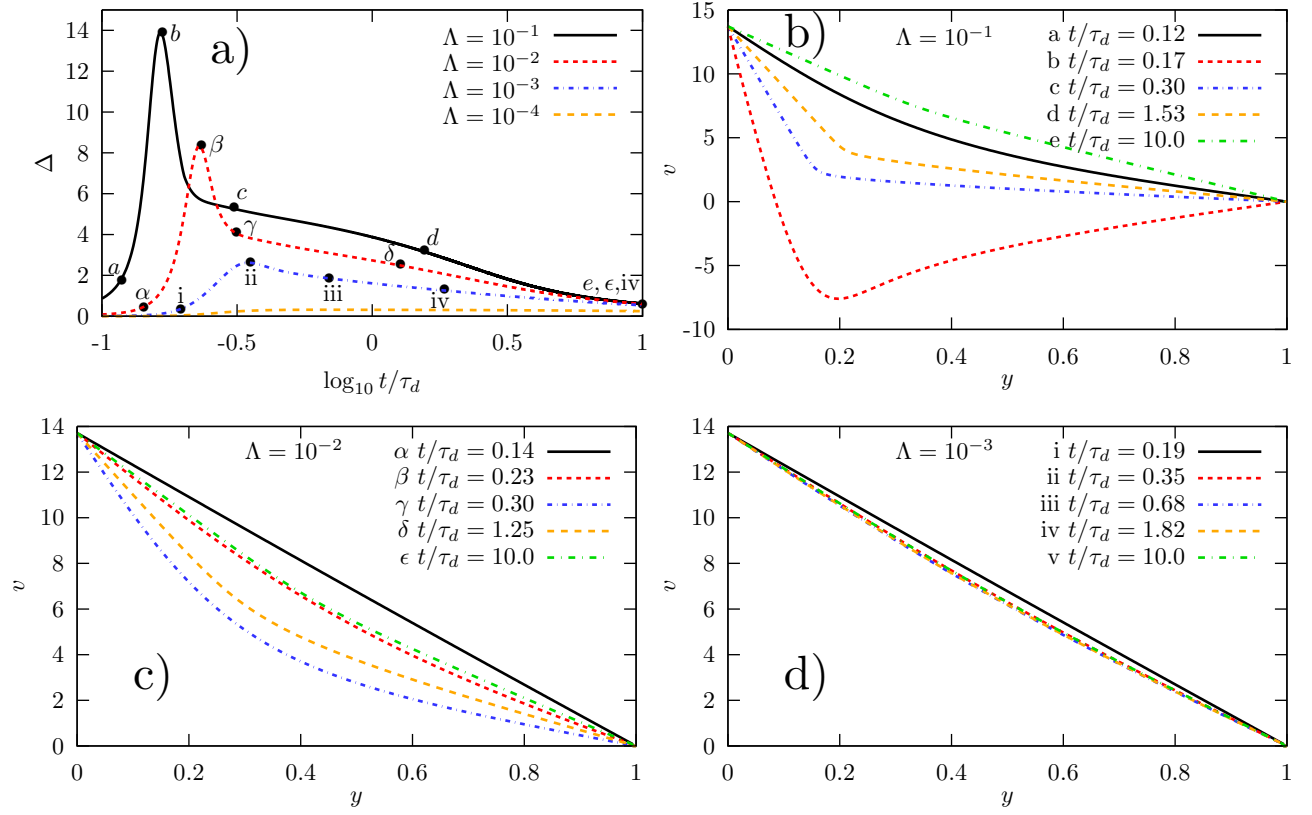


FIG. 7. Effect of noisy initial conditions for  $W_{yy}$  on (a) the shear rate drop  $\Delta$  as a measure of inhomogeneity, and (b-d) transient velocity profiles  $v(y)$ , for different initial conditions  $W_{yy} = \Lambda \cos \pi y$ . In steady state  $W_{yy} = -0.52$ . For parameters  $(\beta, \epsilon, Z) = (0.71, 10^{-5}, 265)$  and  $q = 0$ .

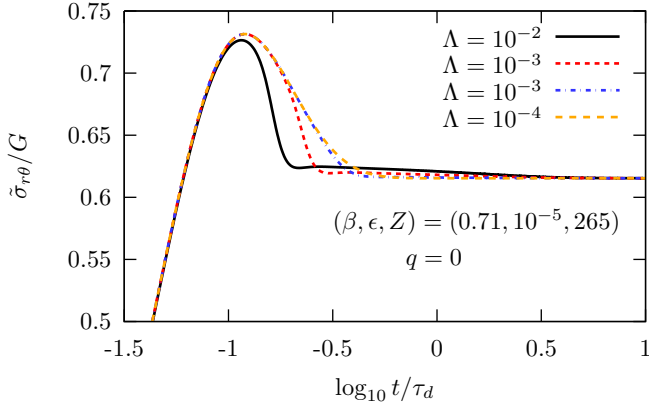


FIG. 8. Stress overshoots for initial conditions  $W_{yy} = \Lambda \cos \pi y$ , parameterized by  $\Lambda$ . For parameters  $(\beta, \epsilon, Z) = (0.71, 10^{-5}, 265)$ .

rates (Tapadia and Wang, 2003). Moreover, the DRP model is only a simple approximation to the more complete GLAMM theory (Likhtman and Graham, 2003; Graham *et al.*, 2003), and there is thus not a precise correspondence between the parameter values used to fit the DRP model to data, and their microscopic physical meaning in the original GLAMM model. For example, we

use rather larger values of entanglement number  $Z$  than are realized in most experiments. However, the DRP model reproduces the qualitative behavior, albeit without the quantitative material parameters. These qualitative conclusions seem to be robust, as far as we can discern: the much broader and flatter steady state constitutive curves are accompanied by dramatic dynamics that can result in transient inhomogeneities. There is an urgent need for performing inhomogeneous calculations with more detailed theories such as the GLAMM model. The GLAMM model itself is also only an approximation, and it certainly misses important physics about the behaviour of the tube at very high shear rates (Graham and McLeish, 2007).

Fig. 11 shows the behavior expected for three values of  $\beta$ , as a function of entanglement number  $Z$  and viscosity ratio  $\epsilon$ , for  $q = 10^{-3}$ . The figure shows regions of (1) steady state banding signified by a non-monotonic constitutive curve; (2) transient banding during startup; and (3) dramatic recoil with negative velocities during startup. From our startup calculations we found these phenomena to occur for shear rate drops (see Eq. 39)  $\Delta \gtrsim 2$  (transient banding) and  $\Delta \gtrsim 7$  (transient banding featuring recoil). Experiments show transient banding for  $Z \sim 15 - 50$ , steady state banding for higher  $Z$ , and recoil for some fluids that do not shear band in steady

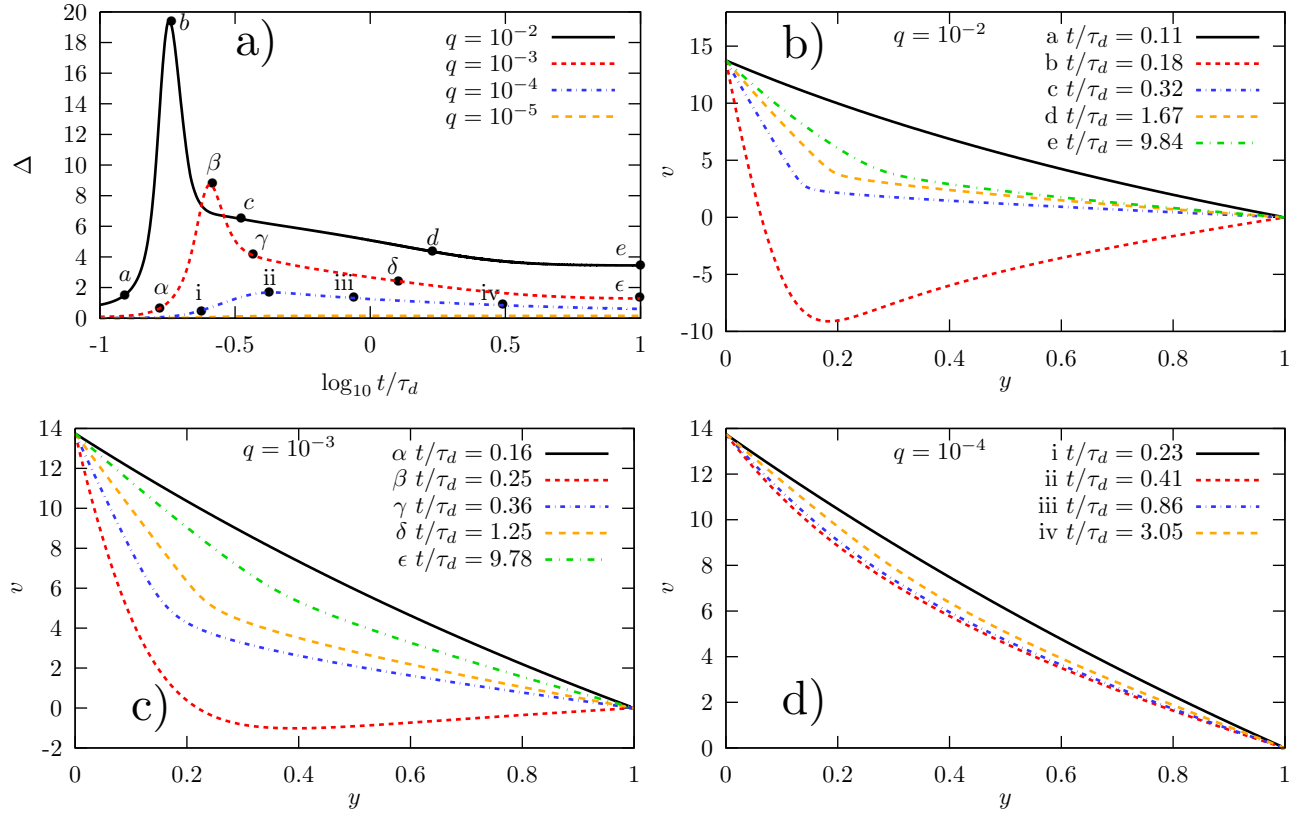


FIG. 9. Effect of different stress gradients  $q \equiv \ln \frac{R_2}{R_1}$  on (a) the shear rate drop  $\Delta$  as a measure of inhomogeneity, and (b-d) transient velocity profiles  $v(y)$ . For parameters  $(\beta, \epsilon, Z) = (0.71, 10^{-5}, 265)$ . The value  $q = 10^{-3}$  corresponds roughly to a cone angle of  $2.5^\circ$ .

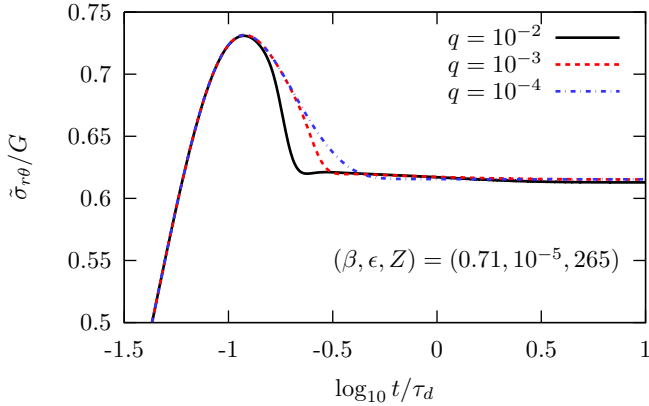


FIG. 10. Stress overshoots for different stress gradients  $q = \ln \frac{R_2}{R_1}$ . For parameters  $(\beta, \epsilon, Z) = (0.71, 10^{-5}, 265)$ .

state. Based on this, we suggest that the experimental phenomenology of entangled polymer solutions most resembles that for values of the CCR parameter  $\beta$  in the range between  $\beta = 0.71$  and  $\beta = 0.8$ , as parametrized by the Rolie-Poly model. We emphasize that the parameter values for this model do not necessarily correspond to those of experiments. However, polymer solutions have a

reasonably wide range of  $Z$  for which transient, and not steady state, banding is found as exhibited in Fig. 11 for  $\beta = 0.71$ .

## B. The stress overshoot and the non-monotonicity of the instantaneous constitutive curve

Fig. 4 shows that transient banding occurs during the decreasing stress after the stress overshoot, and occurs a short time after the unstable eigenvalue is most unstable. At these shear rates the fluid behaves elastically at early times, and the stress overshoot as a function of time could thus be envisioned as the stress overshoot of a *solid* as a function of strain  $\gamma = \dot{\gamma}t$ ; such an elastic material with  $\partial\sigma_{xy}/\partial\gamma < 0$  could be expected to be unstable (Marrucci and Grizzuti, 1983). This was also noted by Sui and McKenna (2007) in their study of entangled polymer solutions

Fig. 6 shows that the integrated instability, as determined by the linear stability analysis, is most pronounced near the flattest part of the constitutive curve. Since the steady state is nearly unstable at this point, it is tempting to declare the nearly flat slope as the cause of the instability. However, the steady state behavior may have little influence on the instantaneous dynamics. To explore



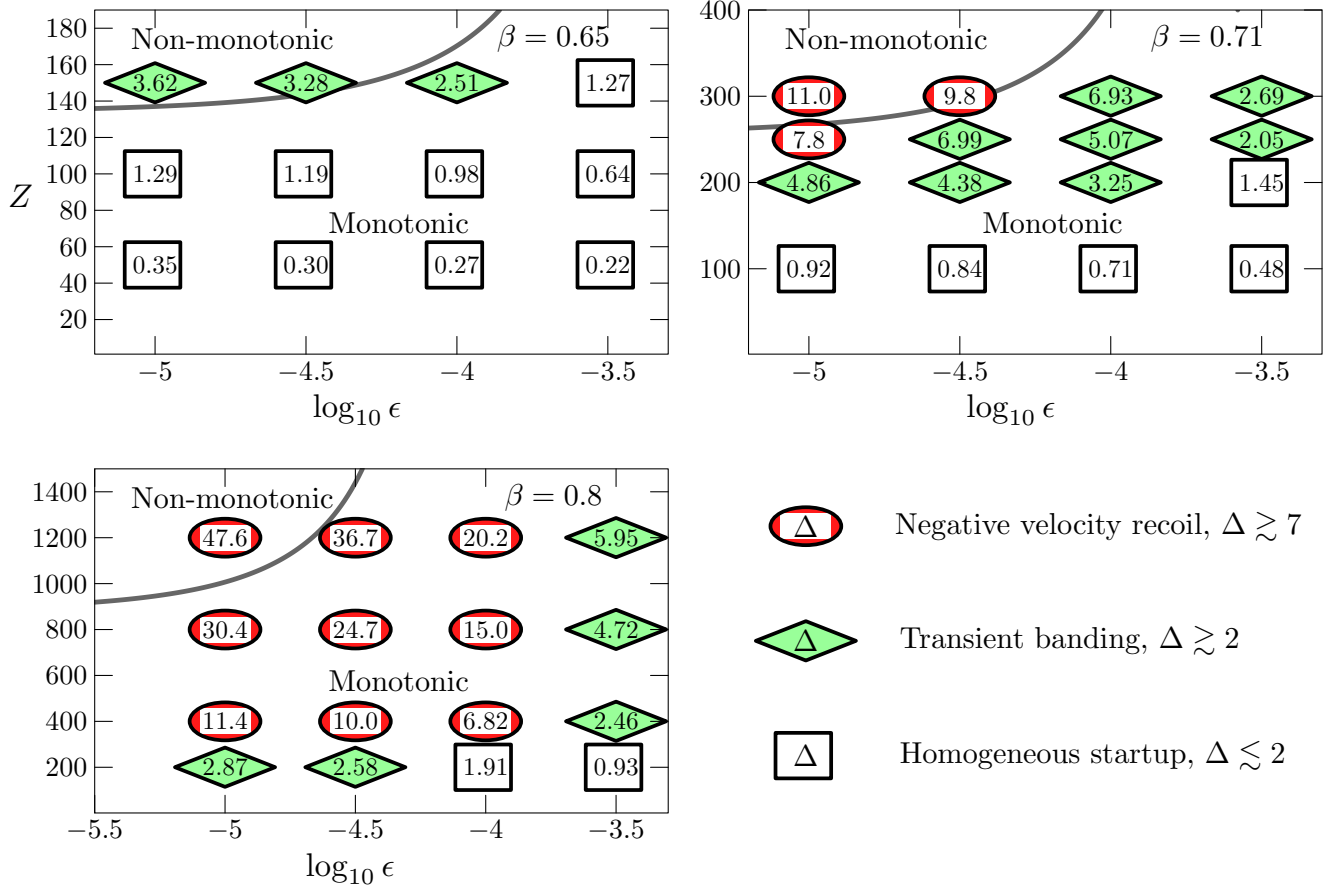


FIG. 11. Regions of parameter space in which one expects to find different phenomena, for  $\beta = 0.65, 0.71, 0.8$  and  $q = 10^{-3}$ . The numbers in boxes denote the largest value of the shear rate drop  $\Delta$  found during startup for an applied average shear rate on the flattest part of the steady state constitutive curve, analogous to the solid circle in Fig. 6. Shown are: steady state banding in the non-monotonic region; transient banding ( $\Delta \gtrsim 2$  and diamonds or ellipses); and negative velocity recoil upon startup ( $\Delta \gtrsim 7$  and ellipses).

this, we have calculated the instantaneous constitutive curve, as described in the introduction and constructed by Hayes *et al.* (2010) from their experimental data. We calculate the startup flow for different *homogeneous* shear rates to obtain a surface  $\sigma_{xy}(\dot{\gamma}, t)$ . This surface then defines a curve relating shear stress to shear rate at any instant in time  $t$  (the *instantaneous constitutive curve*). If this curve has a negative slope, then one expects an instability in the dynamics at finite Reynolds number, or at least in a subspace of the full dynamics specified by the matrix  $\mathbf{M}$  that appears in the linear stability calculation of Section IV A. Fig.12 shows that the instantaneous constitutive curve becomes non-monotonic, with the strongest instability (largest unstable eigenvalue  $\omega_{\max}$ ) indeed occurring very close the point of steepest negative slope  $\partial\sigma_{xy}/\partial\dot{\gamma}$ .

Hence, transient banding, while evidently linked to the steady state constitutive curve, may be expected when the instantaneous constitutive curve is unstable (has negative slope), based on linear stability analysis. It may also be expected during a stress overshoot, for applied

shear rates that approximate a step strain and are thus strong enough to bring the fluid into its elastic regime (Marrucci and Grizzuti, 1983). We emphasize that we have shown a very strong correlation, but in the context of the Rolie-Poly model. The precise correspondences remain to be explored in other models, and we await more work on this subject.

### C. Other transient phenomena

Two other transient banding phenomena have been reported. Well defined shear bands have been observed during portions of the cycle during Large Amplitude Oscillatory Shear (LAOS) in polymer solutions (Tapadia *et al.*, 2006; Ravindranath and Wang, 2008). This has also been calculated numerically by Adams and Olmsted (2009b) using the DRP model for a monotonic constitutive curve, and by Zhou *et al.* (2010) for a non-monotonic constitutive model devised for wormlike micelles. The calculations revealed banding-

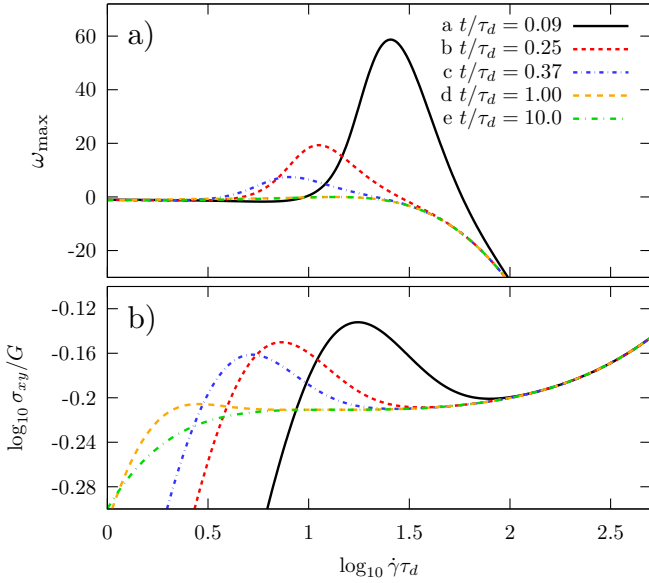


FIG. 12. (a) Maximum eigenvalue as a function of shear rate  $\dot{\gamma}$  for different times  $t$  after startup. (b) instantaneous constitutive curves, calculated from starting up at different shear rates  $\dot{\gamma}$ . Each curve represents the stress obtained a time  $t$  after starting up at the given shear rate  $\dot{\gamma}$ . Note the strong correlation between the region of positive maximum eigenvalue, and the region of negative slope of the time dependent constitutive curve.

like transients for shear rates sweeping across the pseudo-plateau of a barely monotonic constitutive model, and for frequencies slower than the inverse reptation time. This is slow enough for a transient band to form during the upward sweep of strain rate (according to Fig. 4), but not so slow that it decays away completely. It can then be reinforced in subsequent sweeps, given the strong spatial perturbation it represents, until it develops a sharp profile after a few cycles.

In other experiments, step strain at shear rates  $\dot{\gamma} \tau_R > 1$  leads to an inhomogeneous response (including negative velocity recoil) after cessation of step strain, in both solutions (Wang *et al.*, 2006; Ravindranath and Wang, 2007) and melts (Boukany *et al.*, 2009). In one example, a solution of  $Z = 64$  was strained to just the stress maximum in the overshoot. During relaxation, recoil and an inhomogeneous response developed, similar to our previous calculations (Adams and Olmsted, 2009a). One explanation for this result is that the fluid became unstable during strain, and the instability was able to amplify a nascent fluctuation large enough to induce a non-linear and heterogeneous response during the subsequent relaxation. Indeed, the calculation in Fig. 4 shows that the largest eigenvalue can become positive, signifying instability, before the overshoot is reached. However, this cannot be the entire story. In melts the inhomogeneous response can also be a dramatic fracture (Boukany *et al.*, 2009) that, as yet, we cannot calculate from the DRP model (Wang, 2009; Adams and Olmsted, 2009a). This

could be because the DRP model inadequately captures the physics of the GLAMM model; or because important physics governing the heterogeneity associated with retraction has yet to be correctly incorporated in any model (Wang *et al.*, 2007).

#### D. Implications for validating constitutive models

A significant amount of literature, both experimental and theoretical, has been devoted to testing constitutive models against the initial stress transients, including the overshoot and subsequent relaxation (Likhtman and Graham, 2003; Wang *et al.*, 2006). This is typically done by comparing the stress transient for shear rate startup to a calculation that assumes homogeneous shear flow in a planar geometry. As is evident in Fig. 4, the relaxation after the overshoot is faster when the fluid is allowed to become inhomogeneous, as physically occurs during transient banding. Cone and plate geometries are often used because unlimited strains can be applied and the weak stress gradient is usually hoped to be negligible. Unfortunately, the transient banding and hence its associated stress response can be pronounced even for very small stress variations, as parametrized by  $q$ . A planar geometry should exhibit less transient banding if there are no significant perturbations (Fig. 9). We are not yet able to quantify this level of perturbation.

Another common benchmark is the Doi-Edwards damping function  $h(\gamma, t) \equiv \sigma_{xy}(\gamma, t)/\sigma_{xy}(0, t)$ , defined as the stress relaxation  $\sigma_{xy}(\gamma, t)$  after a finite step strain  $\gamma$ , normalized by the relaxation  $\sigma_{xy}(0, t)$  that would occur in the linear limit of zero strain. In strongly entangled systems anomalous behaviour in  $h(\gamma, t)$  has been reported (Osaki, 1993; Venerus, 2005), corresponding to faster relaxation than predicted by DE theory. As noted above, dramatic heterogeneities can also occur during relaxation after a step strain, in the DRP model (Adams and Olmsted, 2009b) and experiments on entangled polymers (Wang *et al.*, 2006; Ravindranath and Wang, 2007; Boukany *et al.*, 2009). These heterogeneities will have a signature in the stress response to a step strain. Thus, it is conceivable that transient heterogeneities could account for the anomalous damping function measurements Marrucci and Grizzuti (1983).

Hence, one must take great care in making predictions for constitutive models: perturbations such as noise or the stress gradients of curved geometries, or the presence of non-monotonic constitutive behavior, necessitates a validation against a full inhomogeneous calculation. This warning was also given by Zhou *et al.* (2008). Such calculations are currently out of reach for models such as the GLAMM model, which already involve solving partial differential equations in time and arc length coordinates (Graham *et al.*, 2003).

## VIII. SUMMARY

Experiments on highly entangled polymers dissolved in their oligomers show inhomogeneous transient velocity profiles in shear flow in a variety of experimental tests. We have modeled this behavior using the single mode diffusive Rolie-Poly (DRP) model. The DRP model has some quantitative shortcomings, but can explain many of the experimental transient phenomena. By varying the model parameters, namely the convective constraint release efficiency  $\beta$ , the entanglement number,  $Z$  and the solvent viscosity  $\epsilon$ , we have shown that transient shear banding can occur even for monotonic constitutive curves. Similar behavior was found by Zhou *et al.* (2008) in calculations using a different non-monotonic model for entangled polymers, the partially extended convective strain model.

A linear stability analysis of the startup transient shows that the homogeneous state is unstable, at early times, to the inhomogeneous transient shear bands. The “weight”  $\Omega_{\max}$  of this instability, given by the time integral of the most unstable eigenvalue, provides a good predictor of flow instability.  $\Omega_{\max}$  is largest where the constitutive curve is flat. If this weight is large then small perturbations can provide the seed for this instability. For large enough perturbations, particularly in fluctuations of the normal stress, the flow profile develops a shear banding state, which then decays over a few relaxation times  $\tau_d$  once the eigenvalue returns to a stable value. We have shown that spatial perturbations play a crucial role in triggering the transient instability. Examples include strong enough stress gradients, as found in rotational rheometers; or inhomogeneous initial conditions due to thermal noise; or residual stress from loading the sample.

Hence, shear banding ranges from the steady state shear banding seen in non-monotonic constitutive curves, to transiently inhomogeneous flow that can develop even for monotonic constitutive curves. The stress overshoot during startup relaxes more quickly, due to the transient shear banding, than if the fluid were to remain homogeneous. This may be consistent with the suggestion long ago by Marrucci and Grizzuti (1983) that an elastic instability could lead to inhomogeneities in a step strain experiment. The relaxation of the stress overshoot is more pronounced in geometries with stronger stress gradients.

Our calculations suggest that fluids with a non-monotonic instantaneous constitutive curve  $\sigma_{xy}(\dot{\gamma}, t)$  are more likely to have an instability and transient banding (Hayes *et al.*, 2010). Indeed, the linear stability analysis in such situations leads to a unstable eigenvalue that is coincident (in time) with the more strongly non-monotonic instantaneous constitutive curves. Similarly, transient banding is strongly correlated with the stress overshoot observed during startup (Sui and McKenna, 2007). This is a subject for future work.

In attempting to fit the parameters of the Rolie-Poly model to the existing data, it is apparent that the model

should be judged mainly for its qualitative conclusions: for example, shear banding in the model occurs for much larger  $Z$  than is found in experiments. The model also fails to describe the high shear rate branch correctly without violating certain physical criteria used to define the effect of stretch on convective constraint release in the parent GLAMM model (Likhtman and Graham, 2003; Graham *et al.*, 2003). Finally, challenges for future work include explaining the dramatic fracture seen in some recent experiments on both entangled melts and solutions (Boukany *et al.*, 2009; Ravindranath and Wang, 2007), and extending (or replacing) the GLAMM model to accurately describe the highest shear rate behavior.

## ACKNOWLEDGMENTS

We are grateful to the UK EPSRC (SMF, EP/E5336X/2) and the Royal Commission of 1851 (JMA) for financial support; and to Ron Larson for useful comments.

- Adams, J. M., Fielding, S. M., and Olmsted, P. D., “The interplay between boundary conditions and flow geometries in shear banding: hysteresis, band configurations, and surface transitions,” *J. Non-Newton. Fl. Mech.* **151**, 101–118 (2008).
- Adams, J. M. and Olmsted, P. D., “Adams and Olmsted reply,” *Phys. Rev. Lett.* **103**, 067801 (2009a).
- Adams, J. M. and Olmsted, P. D., “Nonmonotonic models are not necessary to obtain shear banding phenomena in entangled polymer solutions,” *Phys. Rev. Lett.* **102**, 219802 (2009b).
- Berret, J.-F., “Rheology of wormlike micelles: equilibrium properties and shear banding transition,” in *Molecular Gels*, edited by R. G. Weiss and P. Terech (Springer, Dordrecht, 2005) pp. 235–275.
- Black, W. B. and Graham, M. D., “Wall-slip and polymer-melt flow instability,” *Phys. Rev. Lett.* **77**, 956–959 (1996).
- Boukany, P. E., Hu, Y. T., and Wang, S.-Q., “Observations of wall slip and shear banding in entangled DNA solutions,” *Macromolecules* **41**, 2644–2650 (2008).
- Boukany, P. E., Tapadia, P., and Wang, S. Q., “Interfacial stick-slip transition in simple shear of entangled melts,” *J. Rheol.* **50**, 641–654 (2006).
- Boukany, P. E. and Wang, S.-Q., “A correlation between velocity profile and molecular weight distribution in sheared entangled polymer solutions,” *J. Rheol.* **51**, 217 (2007).
- Boukany, P. E. and Wang, S.-Q., “Exploring the transition from wall slip to bulk shearing banding in well-entangled DNA solutions,” *Soft Matter* **5**, 780–789 (2009a).
- Boukany, P. E. and Wang, S.-Q., “Shear banding or not in entangled DNA solutions depending on the level of entanglement,” *J. Rheol.* **53**, 73 (2009b).
- Boukany, P. E., Wang, S.-Q., and Wang, X., “Step shear of entangled linear polymer melts: New experimental evidence for elastic yielding,” *Macromolecules* **42**, 6261–6269 (2009).
- Cates, M. E., “Nonlinear viscoelasticity of wormlike micelles (and other reversibly breakable polymers),” *J. Phys. Chem.* **94**, 371–375 (1990).
- Cates, M. E. and Fielding, S. M., “Rheology of giant micelles,” *Adv. Physics* **55**, 799–879 (2006).
- Crawley, R. L. and Graessley, W. W., “Geometry effects on stress transient data obtained by cone and plate flow,” *J. Rheology* **21**, 19–49 (1977).
- Denn, M. M., “Extrusion instabilities and wall slip,” *Ann. Rev. Fl. Mech.* **33**, 265–287 (2001).

- Divoux, T., Tamarii, D., Barentin, C., and Manneville, S., "Transient shear banding in a simple yield stress fluid," *Phys. Rev. Lett.* **104**, 208301 (2010).
- Doi, M. and Edwards, S. F., *The Theory of Polymer Dynamics* (Clarendon, Oxford, 1989).
- Doi, M. and Edwards, S. F., "Dynamics of concentrated polymer systems. Part 4.—Rheological properties," *J. Chem. Soc., Far. Trans. 2* **75**, 38–54 (1979).
- Fielding, S. M. and Olmsted, P. D., "Kinetics of the shear banding instability in startup flows," *Phys. Rev. E* **68**, 036313 (2003).
- Fukuda, M., Osaki, K., and Kurata, M., "Nonlinear viscoelasticity of polystyrene solutions. I. Strain-dependent relaxation modulus," *J. Polym. Sci. Polym. Phys.* **13**, 1563–1576 (1975).
- Graham, R. S., Likhtman, A. E., McLeish, T. C. B., and Milner, S. T., "Microscopic theory of linear, entangled polymer chains under rapid deformation including chain stretch and convective constraint release," *J. Rheol.* **47**, 1171–1200 (2003).
- Graham, R. S. and McLeish, T. C. B., "Emerging applications for models of molecular rheology," *J. Non-Newt. Fl. Mech.* **150**, 11–18 (2007).
- Greco, F. and Ball, R. C., "Shear-band formation in a non-Newtonian fluid model with a constitutive instability," *J. Non-Newt. Fl. Mech.* **69**, 195–206 (1997).
- Hayes, K. A., Buckley, M. R., Qi, H., Cohen, I., and Archer, L. A., "Constitutive curve and velocity profile in entangled polymers during start-up of steady shear flow," *Macromolecules* **43**, 4412–4417 (2010).
- Hu, Y. T., Palla, C., and Lips, A., "Comparison between shear banding and shear thinning in entangled micellar solutions," *J. Rheol.* **52**, 379–400 (2008a).
- Hu, Y. T., Palla, C., and Lips, A., "Role of Electrostatic Interactions in Shear Banding of Entangled DNA Solutions," *Macromolecules* **41**, 6618–6620 (2008b).
- Hu, Y. T., Wilen, L., Philips, A., and Lips, A., "Is the constitutive relation for entangled polymers monotonic?," *J. Rheol.* **51**, 275 (2007).
- Islam, M. T. and Archer, L. A., "Nonlinear rheology of highly entangled polymer solutions in start-up and steady shear flow," *J. Polym., Sci. Part B* **39**, 2275–2289 (2001).
- Jagla, E. A., "Towards a modeling of the time dependence of contact area between solid bodies," *J. Stat.Mech.* **2010**, P06006 (2010).
- Kolkka, R. W., Malkus, D. S., Hansen, M. G., and Ierley, G. R., "Spurt phenomena of the Johnson-Segalman fluid and related models," *J Non-Newt. Fl. Mech.* **29**, 303–335 (1988).
- Larson, R. G., "A constitutive equation for polymer melts based on partially extending strand convection," *J. Rheol.* **28**, 545–571 (1984).
- Larson, R. G., *The Structure and Rheology of Complex Fluids* (Oxford University Press, New York, 1999).
- Larson, R. G., Sridhar, T., Leal, L. G., McKinley, G. H., Likhtman, A. E., and McLeish, T. C. B., "Definitions of entanglement spacing and time constants in the tube model," *J. Rheol.* **47**, 809 (2003).
- Likhtman, A. E. and Graham, R. S., "Simple constitutive equation for linear polymer melts derived from molecular theory: Rolie-poly equation," *J. Non-Newt. Fl. Mech.* **114**, 1 (2003).
- Likhtman, A. E., Milner, S. T., and McLeish, T. C. B., "Microscopic theory for the fast flow of polymer melts," *Phys. Rev. Lett.* **85**, 4550–4553 (2000).
- Lu, C-Y. D., Olmsted, P. D., and Ball, R. C., "The effect of non-local stress on the determination of shear banding flow," *Phys. Rev. Lett.* **84**, 642–645 (2000).
- Manning, M. L., Daub, E. G., Langer, J. S., and Carlson, J. M., "Rate-dependent shear bands in a shear-transformation-zone model of amorphous solids," *Phys. Rev. E* **79**, 016110 (2009).
- Manning, M. L., Langer, J. S., and Carlson, J. M., "Strain localization in a shear transformation zone model for amorphous solids," *Phys. Rev. E* **76**, 056106 (2007).
- Marrucci, G., "Dynamics of entanglements. a nonlinear model consistent with cox-merz rule," *J. Non-Newtonian Fluid Mech* **62**, 279 (1996).
- Marrucci, G. and Grizzuti, N., "The free energy function of the Doi-Edwards theory: analysis of the instabilities in stress relaxation," *J. Rheol.* **27**, 433 (1983).
- McLeish, T. C. B. and Ball, R. C., "A molecular approach to the spurt effect in polymer melt flow," *J. Poly. Sci. B-Poly. Phys.* **24**, 1735–1745 (1986).
- Mead, D. W., Larson, R. G., and Doi, M., "A molecular theory for fast flows of entangled polymers," *Macromolecules* **31**, 7895–7914 (1998).
- Menezes, E. V. and Graessley, W. W., "Nonlinear rheological behavior of polymer systems for several shear-flow histories," *J. Polym. Sci.: Polym. Phys.* **20**, 1817–1833 (1982).
- Milner, S. T., McLeish, T. C. B., and Likhtman, A. E., "Microscopic theory of convective constraint release," *J. Rheol.* **45**, 539–563 (2001).
- Moorcroft, R. L., Cates, M. E., and Fielding, S. M., "Age-dependent transient shear banding in soft glasses," *Phys. Rev. Lett.* **106**, 055502 (2011).
- Morrison, F. A. and Larson, R. G., "A study of shear-stress relaxation anomalies in binary-mixtures of monodisperse polystyrenes," *J. Polym. Sci. Part B-Polym. Phys.* **30**, 943–950 (1992).
- Olmsted, P. D., "Perspectives on shear banding in complex fluids," *Rheol. Acta* **47**, 283–300 (2008).
- Olmsted, P. D., Radulescu, O., and Lu, C-Y. D., "The Johnson-Segalman model with a diffusion term in cylindrical Couette flow," *J. Rheology* **44**, 257–275 (2000).
- Osaki, K., "On the damping function of shear relaxation modulus for entangled polymers," *Rheol. Acta* **32**, 429–437 (1993).
- Osaki, K. and Kurata, M., "Experimental appraisal of the Doi-Edwards theory for polymer rheology based on the data for polystyrene solutions," *Macromolecules* **13**, 671–676 (1980).
- Ravindranath, S. and Wang, S.-Q., "What are the origins of stress relaxation in step shear of entangled polymer solutions?," *Macromolecules* **40**, 8031–8029 (2007).
- Ravindranath, S. and Wang, S.-Q., "Large amplitude oscillatory shear behavior of entangled polymer solutions: Particle tracking velocimetric investigation," *J. Rheol.* **52**, 341 (2008).
- Ravindranath, S., Wang, S.-Q., Olechnowicz, M., and Quirk, R. P., "Banding in simple steady shear of entangled polymer solutions," *Macromolecules* **41**, 2663–2670 (2008).
- Rehage, H. and Hoffmann, H., "Viscoelastic surfactant solutions: model systems for rheological research," *Mol. Phys.* **74**, 933 (1991).
- Rossi, L. F., McKinley, G., and Cook, L. P., "Slippage and migration in taylor-couette flow of a model for dilute wormlike micellar solutions," *J. Non-Newt. Fl. Mech.* **136**, 79 (2006).
- Spenley, N. A., Cates, M. E., and McLeish, T. C. B., "Nonlinear rheology of wormlike micelles," *Phys. Rev. Lett.* **71**, 939–942 (1993).
- Sui, C. and McKenna, G. B., "Instability of entangled polymers in cone and plate rheometry," *Rheol. Acta* **46**, 877–888 (2007).
- Tapadia, P., Ravindranath, S., and Wang, S.-Q., "Banding in entangled polymer fluids under oscillatory shearing," *Phys. Rev. Lett.* **96**, 196001 (2006).
- Tapadia, P. and Wang, S.-Q., "Yieldlike constitutive transition in shear flow of entangled polymeric fluids," *Phys. Rev. Lett.* **91**, 198301 (2003).
- Tapadia, P. and Wang, S.-Q., "Nonlinear flow behavior of entangled polymer solutions: Yieldlike entanglement-disentanglement transition," *Macromolecules* **37**, 9083–9095 (2004).
- Tapadia, P. and Wang, S.-Q., "Direct visualization of continuous simple shear in non-newtonian polymeric fluids," *Phys. Rev. Lett.* **96**, 016001 (2006).
- Venerus, D.C., "A critical evaluation of step strain flows of entangled linear polymer liquids," *Journal of Rheology* **49**, 277–295 (2005).



- Venerus, D.C. and Nair, R., "Stress relaxation dynamics of an entangled polystyrene solution following step strain flow," *Journal of rheology* **50**, 59–75 (2006).
- Vinogradov, G. V., "Critical regimes of deformation of liquid polymeric systems," *Rheol. Acta* **12**, 273 (1973).
- Vrentas, C. M. and Graessley, W. W., "Study of shear stress relaxation in well-characterized polymer liquids," *J. Rheol.* **26**, 359–371 (1982).
- Wang, S. Q., "Molecular transitions and dynamics at polymer/wall interfaces: Origins of flow instabilities and wall slip," in *Polymers in Confined Environments*, Adv. Poly. Sci., Vol. 138 (Springer, Berlin, 1999) pp. 227–275.
- Wang, S.-Q., "Comment on "nonmonotonic models are not necessary to obtain shear banding phenomena in entangled polymer solutions"," *Phys. Rev. Lett.* **103**, 219801 (2009).
- Wang, S.-Q., Ravindranath, S., Boukany, P., Olechnowicz, M., Quirk, R., Halasa, A., and Mays, J., "Nonquiescent relaxation in entangled polymer liquids after step shear," *Phys. Rev. Lett.* **97**, 187801 (2006).
- Wang, S.-Q., Ravindranath, S., Wang, Y., and Boukany, P., "New theoretical consideration in polymer rheology: Elastic breakdown of chain entanglement network liquid state," *J. Chem. Phys.* **127**, 064903 (2007).
- Zhou, L., Cook, L. P., and McKinley, G. H., "Probing shear-banding transitions of the vcm model for entangled wormlike micelle model for entangled wormlike micellar solutions using large amplitude oscillatory shearing (LAOS) deformation," *J. Non-Newt. Fl. Mech.* **165**, 1462–1472 (2010).
- Zhou, L., Vasquez, P. A., Cook, L. P., and McKinley, G. A., "Modeling the inhomogeneous response and formation of shear bands in steady and transient flows of entangled liquids," *J. Rheol.* **52**, 591–623 (2008).